AIAA JOURNAL
Vol. 30, No. 10, October 1992

Flutter of Composite Laminated Beam Plates with Delamination

Le-Chung Shiau*
National Cheng Kung University, Tainan, Taiwan, Republic of China

The flutter characteristics of two-dimensional delaminated composite panels at high supersonic Mach numbers are investigated theoretically. Classical small deflection laminated plate theory and quasisteady, supersonic aerodynamic theory are employed. A simple beam-plate theory model is developed to predict the flutter boundaries of delaminated composite two-dimensional beam plates with simply supported ends. The effects of delamination position and size on the flutter boundary of plate with different fiber orientation and stacking sequency are studied in detail. The results reveal that the presence of a delamination degrades the stiffness and the natural frequencies of the plate and thereby decreases the flutter boundary of the plate. However, for certain geometries, the flutter boundaries were raised due to the flutter coalescence modes of the plate altered by the presence of a delamination in the plate. The restriction in the two-dimensional beam-plate model is to evaluate the effects of delamination on the flutter boundary for a two-dimensional plate only. But the trends of the effects of delamination on composite panel flutter can be evaluated for comparison purpose using this theory.

Nomenclature

A_i = extensional stiffness of segment i
a = plate length
a_i = location of delamination edges
B_i = coupling stiffness of segment i
b_n = see Eq. (6)
C_{jn} = constant of integration
$\bar{c}$ = location of delamination
D_i = bending stiffness of segment i
$\bar{d}$ = delamination length
E_1, E_2 = Young's moduli referred to principal material directions
F = contact force between segments 2 and 3
G_{12} = shear modulus
g = aerodynamic damping
H = see Eq. (9)
h_i = plate thickness of segment i
K, q = see Eq. (8)
M = bending moment in plate
M_ω = Mach number
N = number of layers of plate
P_i = in-plane forces in segments 2 and 3
Q_{ij} = transformed reduced stiffness
s_i = a_i/a
t = time
U = air velocity
u = in-plane displacement
V = shear force in plate
W = nondimensional plate deflection
w = plate deflection
x = distance along length
Z = mathematical eigenvalue
$\gamma, \delta, \epsilon, \bar{\gamma}, \bar{\delta}, \bar{\epsilon}$ = see Eqs. (10) and (11)
Δp = aerodynamic pressure
κ = nondimensional frequency
λ = nondimensional dynamic pressure
ν = Poisson's ratio
ξ = x/a
ρ = air density
ρ_m = plate density
ω = frequency
ω_n = fundamental natural frequency

Subscripts

i = imaginary
k = layer number
n = segment number
r = real

Introduction

COMPOSITE materials have been widely used in aeronautical industries to replace metals in the aircraft structures for the purpose of weight saving. With their superior strength-to-weight and stiffness-to-weight ratios and the capability of being tailored for a specific application, composite materials offer definite advantages over conventional materials. But to use them efficiently, a good understanding of their structural and dynamic behaviors under various loads is needed. One important issue in the evaluation of laminated composite structures is interlaminar delamination between the composite layers. Delaminations may be caused by impact damages from fabrication defects or service. Hence, the delamination can be located in various places in the laminated plate. Regardless of its location, delamination may reduce the overall stiffness of the laminate, lower the load-carrying capacity of the plate, and, thereby, affect the mechanical behavior of the structural system. The effects of delamination on the structural behavior of composite laminates have received much attention in recent years.[1-3] In the study of delamination effects on the natural frequencies of composite laminates, Tracy and Pardoen[1] found that the delamination position and size have moderate effects on the natural frequencies. The presence of a delamination degrades the even-numbered symmetric vibration modes much more rapidly than the odd-numbered antisymmetric modes for a delamination centered at the plate midplane.

Panel flutter is a self-excited oscillation of the external skin of a flight vehicle and is due to dynamic instability of inertia, elastic, and aerodynamic forces of the system. This type of aeroelastic instability has received much attention in the past 30 years.[4-15] As a result, this peculiar phenomenon is now reasonably understood for two- and three-dimensional panels made of conventional isotropic materials. However, relatively few works have been devoted to the study of the flutter characteristics of panels made of advanced composite materi-

Received Aug. 21, 1991; revision received Feb. 24, 1992; accepted for publication March 1, 1992.

*Professor, Institute of Aeronautics and Astronautics.

als.[16-20] In panel flutter analysis, the determination of the occurrence of aeroelastic instability is through the coupling of natural modes of the system. As the delamination degrades the natural modes of a delaminated laminate, it may have significant effects on the flutter behavior of the laminate. In the present study, a simple beam-plate model is developed for the preliminary investigation of the effect of delamination on the supersonic flutter behavior of composite laminated panels. Classic small deflection laminated plate theory and quasi-steady aerodynamic theory are employed for the analysis. The effects of delamination size and position in determining flutter boundary are examined. Results are presented for flutter boundary of the delaminated panels as functions of the position and size of the delamination and the fiber orientation and stacking sequency of the laminates.

Mathematical Formulation

Consider a two-dimensional symmetrical laminated thin plate with length a, thickness h, and mass density per unit volume ρ_m as shown in Fig. 1. The plate is assumed to consist of N layers of homogeneous anisotropic sheets bonded together and to have a through width delamination with length $\bar{d}$. The center of the delamination is located at a distance $\bar{c}$ from the left edge. Supersonic airflow with air density ρ, flow velocity U, Mach number M_∞, and aerodynamic pressure Δp is assumed to pass over the top surface of the plate along the positive x direction.

The delaminated beam plate can be divided into four segments as depicted in Fig. 1 and denoted as circled numbers. The lateral deflection of the plate is assumed to be small so that classical small deflection plate theory is adequate to describe the plate's behavior; thus, the governing differential equations of motion for each segment are

$$D_1\frac{\partial^4 w_1}{\partial x^4}+\rho_m h_1\frac{\partial^2 w_1}{\partial t^2}+\Delta p=0 \tag{1a}$$

$$D_2\frac{\partial^4 w_2}{\partial x^4}-B_2\frac{\partial^3 u_2}{\partial x^3}-P_2\frac{\partial^2 w_2}{\partial x^2}+\rho_m h_2\frac{\partial^2 w_2}{\partial t^2}+\Delta p+F=0 \tag{1b}$$

$$D_3\frac{\partial^4 w_3}{\partial x^4}-B_3\frac{\partial^3 u_3}{\partial x^3}-P_3\frac{\partial^2 w_3}{\partial x^2}+\rho_m h_3\frac{\mathrm{d}^2 w_3}{\partial t^2}-F=0 \tag{1c}$$

$$D_4\frac{\partial^4 w_4}{\partial x^4}+\rho_m h_4\frac{\partial^2 w_4}{\partial t^2}+\Delta p=0 \tag{1d}$$

$$P_2=A_2\frac{\partial u_2}{\partial x}-B_2\frac{\partial^2 w_2}{\partial x^2} \tag{1e}$$

$$P_3=A_3\frac{\partial u_3}{\partial x}-B_3\frac{\partial^2 w_3}{\partial x^2} \tag{1f}$$

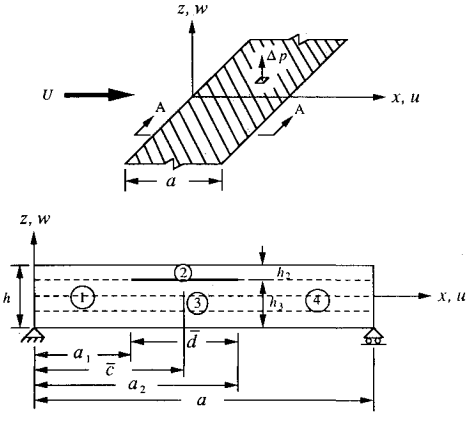

Fig. 1 Plate geometry.

in which w_n ($n=1, 2, 3, 4$) is the lateral displacement of the plate, F is the contact force between segments 2 and 3, P_n ($n=2, 3$) is the in-plane force induced by the delamination, u_n ($n=2, 3$) is the uniform in-plane displacement of the plate, and

$$A_n=\sum_{k=i}^{m}(\bar{Q}_{11})_k(z_k-z_{k-1}) \quad i=\begin{cases}1 & \text{for } n=1,3,4\\ j+1 & \text{for } n=2\end{cases}$$

$$B_n=\frac{1}{2}\sum_{k=i}^{m}(\bar{Q}_{11})_k(z_k^2-z_{k-1}^2) \quad m=\begin{cases}N & \text{for } n=1,2,4\\ j & \text{for } n=3\end{cases}$$

$$D_n=\frac{1}{3}\sum_{k=i}^{m}(\bar{Q}_{11})_k(z_k^3-z_{k-1}^3)$$

where $(\bar{Q}_{11})_k$ is the x-direction transformed reduced stiffness of the kth layer and the other Q_{ij} ($i, j=2, 3$) are neglected in this two-dimensional formulation.

Equation (1) is a highly nonlinear equation due to the contact/uncontact phenomenon between segments 2 and 3. According to a study by Tracy and Pardoen,[1] the natural frequencies of a delaminated beam plate can be accurately predicted by a simplified analytical model that assumes that the two delaminated segments are forced to vibrate together. For the prediction of flutter boundary of a delaminated beam plate, it is also assumed, in this study, that the segments 2 and 3 are forced to vibrate together (i.e., the contact force can be either positive or negative). Under this assumption and with $P_2+P_3=0$ condition, Eq. (1) can be simplified as

$$D_1\frac{\partial^4 w_1}{\partial x^4}+\rho_m h_1\frac{\partial^2 w_1}{\partial t^2}+\Delta p=0 \tag{2a}$$

$$\left(D_2+D_3-\frac{B_2^2}{A_2}-\frac{B_3^2}{A_3}\right)\frac{\partial^4 w_2}{\partial x^4}+\rho_m(h_2+h_3)\frac{\partial^2 w_2}{\partial t^2}+\Delta p=0 \tag{2b}$$

$$D_4\frac{\partial^4 w_4}{\partial x^4}+\rho_m h\frac{\partial^2 w_4}{\partial t^2}+\Delta p=0 \tag{2c}$$

$$P_2=A_2\frac{\partial u_2}{\partial x}-B_2\frac{\partial^2 w_2}{\partial x^2} \tag{2d}$$

For high supersonic Mach numbers ($M_\infty>1.6$), the aerodynamic pressure loading Δp is assumed to follow two-dimensional quasisteady supersonic piston aerodynamic theory:

$$\Delta p=\frac{\rho U^2}{\sqrt{M_\infty^2-1}}\left(\frac{\partial w_n}{\partial x}+\frac{M_\infty^2-2}{M_\infty^2-1}\frac{1}{U}\frac{\partial w_n}{\partial t}\right) \text{ for } n=1, 2, 4 \tag{3}$$

Assuming the displacements for each segment of the plate are exponential (harmonic) functions of time, $w_n=\bar{w}_n(x)e^{i\omega t}$, and introducing the following nondimensional parameters and constants,

$$W_n=\bar{w}_n/h \quad \xi=x/a \quad c=\bar{c}/a \quad d=\bar{d}/a$$

$$\lambda=\frac{\rho U^2 a^3}{\sqrt{M_\infty^2-1}D} \quad g=\frac{\rho U}{M_\infty\rho_m h\omega_0} \quad k=\omega/\omega_0$$

$$\omega_0=\pi^2\sqrt{\frac{D}{\rho_m h a^4}} \quad s_1=a_1/a \quad s_2=a_2/a$$

$$\bar{D}_1=D_1/D \quad \bar{D}_4=D_4/D \quad \bar{D}=\frac{D_2+D_3}{D}-\frac{B_2^2}{DA_2}-\frac{B_3^2}{DA_3}$$

Eqs. (2) and (3) can be nondimensionalized and combined into one equation as

$$\bar{D}_1\frac{\partial^4 W_1}{\partial\xi^4}+\lambda\frac{\partial W_1}{\partial\xi}+\pi^4(ikg-k^2)W_1=0 \tag{4a}$$

$$\bar{D}\frac{\partial^4 W_2}{\partial\xi^4}+\lambda\frac{\partial W_2}{\partial\xi}+\pi^4(ikg-k^2)W_2=0 \tag{4b}$$

$$\bar{D}_4\frac{\partial^4 W_4}{\partial\xi^4}+\lambda\frac{\partial W_4}{\partial\xi}+\pi^4(ikg-k^2)W_4=0 \tag{4c}$$

in which λ is the nondimensional aerodynamic pressure, k is the nondimensional frequency, and D is the bending stiffness of the plate when all fibers are aligned with the x axis.

The solutions to Eq. (4) have the following form:

$$W_n=\sum_{j=1}^{4}C_{jn}e^{b_{jn}\xi}\qquad \text{for}\quad n=1,2,4 \tag{5}$$

where the b_{jn} are the roots of the polynomials

$$\bar{D}_1 b_n^4+\lambda b_n-\pi^4 Z=0\qquad \text{for}\quad n=1,4 \tag{6a}$$

$$\bar{D} b_n^4+\lambda b_n-\pi^4 Z=0\qquad \text{for}\quad n=2 \tag{6b}$$

and

$$Z=k^2-ikg \tag{6c}$$

Equation (5) possesses 12 unknown constants so that 12 boundary and continuity conditions are required. For the two-dimensional panel with simply supported edges, the boundary conditions, both in-plane and transverse, and the continuity conditions are as follows:

1) Transverse simply supported boundary conditions:

$$\text{at}\quad x=0:\qquad w_1(0)=\frac{\partial^2 w_1(0)}{\partial x^2}=0 \tag{7a}$$

$$\text{at}\quad x=a:\qquad w_4(a)=\frac{\partial^2 u_4(a)}{\partial x^2}=0 \tag{7b}$$

2) Kinematic continuity conditions:

$$\text{at}\quad x=a_1:\qquad w_1(a_1)=w_2(a_1) \tag{7c}$$

$$\frac{\partial w_1(a_1)}{\partial x}=\frac{\partial w_2(a_1)}{\partial x} \tag{7d}$$

$$\text{at}\quad x=a_2:\qquad w_2(a_2)=w_4(a_2) \tag{7e}$$

$$\frac{\partial w_2(a_2)}{\partial x}=\frac{\partial w_4(a_2)}{\partial x} \tag{7f}$$

3) Continuity in bending moments and shear forces:

$$\text{at}\quad x=a_1:\qquad V_1(a_1)=V_2(a_1)+V_3(a_1) \tag{7g}$$

$$M_1(a_1)=M_2(a_1)+M_3(a_1) \tag{7h}$$

$$\text{at}\quad x=a_2:\qquad V_4(a_2)=V_2(a_2)+V_3(a_2) \tag{7i}$$

$$M_4(a_2)=M_2(a_2)+M_3(a_2) \tag{7j}$$

in which the shear force $V_i=(B_i^2/A_i-D_i)\,\partial^3 w_i/\partial x^3$ and the bending moment $M_i=B_iP_i/A_i+(B_i^2/A_i-D_i)\,\partial^2 w_i/\partial x^2$.

Besides, one additional in-plane compatibility condition at $x=a_2$ is required to eliminate P_2 from the previous 12 conditions. From Eqs. (1e) and (1f), we can derive the following equation:

$$\frac{P_2}{A_2}(a_2-a_1)+\frac{B_2}{A_2}\left[\frac{\partial w_2(a_2)}{\partial x}-\frac{\partial w_2(a_1)}{\partial x}\right]=\frac{P_3}{A_3}(a_2-a_1)+\frac{B_3}{A_3}\left[\frac{\partial w_3(a_2)}{\partial x}-\frac{\partial w_3(a_1)}{\partial x}\right]$$

or

$$P_2=\frac{A_2B_3-A_3B_2}{(a_2-a_1)(A_2+A_3)}\left[\frac{\partial w_2(a_2)}{\partial x}-\frac{\partial w_2(a_1)}{\partial x}\right] \tag{7k}$$

Satisfaction of the boundary and continuity conditions by substituting Eq. (5) into Eq. (7) yields 12 homogeneous, linear algebraic equations in the unknowns C_{jn},

$$[K]_{12\times 12}\{q\}_{12\times 1}=\{0\}_{12\times 1} \tag{8}$$

where K_{ij} are the coefficients of the unknown constants and $\{q\}$ is the column vector containing the 12 unknown constants: C_{11}, C_{21}, C_{31}, C_{41}, C_{12}, C_{22}, C_{32}, C_{42}, C_{14}, C_{24}, C_{34}, and C_{44}. The 144 K_{ij} coefficients are given in the Appendix.

For a nontrivial solution to exist, the determinant of the coefficient matrix $[K]$ must equal to zero, which gives the characteristic equation for the eigenvalues. The functional relation may be expressed as

$$H(\lambda, Z)=0 \tag{9}$$

Solution Procedures

The four roots of Eq. (6a) are assumed in the form of

$$b_1=-\gamma+\epsilon\qquad b_2=-\gamma-\epsilon \tag{10a}$$

$$b_3=\gamma+i\delta\qquad b_4=\gamma-i\delta \tag{10b}$$

and the four roots of Eq. (6b) are in the form of

$$\bar{b}_1=-\bar{\gamma}+\bar{\epsilon}\qquad \bar{b}_2=-\bar{\gamma}-\bar{\epsilon} \tag{11a}$$

$$\bar{b}_3=\bar{\gamma}+i\bar{\delta}\qquad \bar{b}_4=\bar{\gamma}-i\bar{\delta} \tag{11b}$$

Placing Eqs. (10) and (11) into Eqs. (6), one obtains

$$\delta^2=\frac{\lambda}{4\gamma\bar{D}_1}+\gamma^2\qquad \bar{\delta}^2=\frac{\lambda}{4\bar{\gamma}\bar{D}}+\bar{\gamma}^2 \tag{12a}$$

$$\epsilon^2=\frac{\lambda}{4\gamma\bar{D}_1}-\gamma^2\qquad \bar{\epsilon}^2=\frac{\lambda}{4\bar{\gamma}\bar{D}}-\bar{\gamma}^2 \tag{12b}$$

$$Z=\frac{\bar{D}_1}{\pi^4}(\gamma^2+\delta^2)(-\gamma^2+\epsilon^2)=\frac{\bar{D}}{\pi^4}(\bar{\gamma}^2+\bar{\delta}^2)(-\bar{\gamma}^2+\bar{\epsilon}^2) \tag{12c}$$

Manipulating Eq. (12) yields one cubic equation in γ^2 and one in $\bar{\gamma}^2$ with λ and Z as parameters

$$64\gamma^6+\frac{16\pi^4 Z}{\bar{D}_1}\gamma^2-\frac{\lambda^2}{\bar{D}_1^2}=0 \tag{13a}$$

$$64\bar{\gamma}^6+\frac{16\pi^4 Z}{\bar{D}}\bar{\gamma}^2-\frac{\lambda^2}{\bar{D}^2}=0 \tag{13b}$$

For a given λ and Z, the values of γ, $\bar{\gamma}$, δ, $\bar{\delta}$, ϵ, and $\bar{\epsilon}$ are calculated in turn from Eqs. (13) and (12), and the eight roots in Eqs. (10) and (11) can then be determined. Finally, the complex function H is evaluated from Eq. (9). In general, H will not be zero, so another value of Z is chosen for the fixed λ and H is recomputed until a zero of H is obtained with acceptable accuracy. In the present calculations, this is three significant figures for both complex and real roots.

Once the eigenvalues Z of the characteristic equation are obtained, the frequencies of the plate may be computed from Eq. (6c) or

$$\omega/\omega_0=ig/2\pm\sqrt{-(g/2)^2+Z} \tag{14}$$

For low values of λ, the eigenvalues Z are real, but above a certain value of λ, the Z become complex. After the eigenvalues become complex, unstable conditions will occur if the imaginary part of the radical in Eq. (14) has an absolute value greater than $g/2$. The imaginary part of the radical can be obtained as

$$\text{Im}=\pm\frac{1}{\sqrt{2}}\sqrt{\sqrt{(-g^2/4+Z_r)^2+Z_i^2}+g^2/4-Z_r} \tag{15}$$

Hence, instability occurs when $g/2 = |\mathrm{Im}|$, or, by routine algebraic manipulation, the flutter condition occurs at the critical value of $\lambda = \lambda_{cr}$ when

$$Z_i/\sqrt{Z_r} = g \tag{16}$$

For the case neglecting aerodynamic damping, $g = 0$, flutter will begin after two undamped natural frequencies have merged. For some damping present, $g > 0$, the flutter occurs at a somewhat higher value of λ.

The solution procedures used here represent an exact solution rather than a modal solution of the differential equation and hence do not possess convergence difficulties.

Numerical Results

The two-dimensional panels considered for this study are four-layer angle-ply and cross-ply symmetrical laminated plates and a $[(90, \pm 45, 0)_2]_{sym}$ general laminate that is frequently employed in current aerospace designs. The material properties of the laminates are for a typical high modulus Hercules AS4/3501-6 graphite-epoxy composite system with $E_1 = 13.643E_2$, $G_{12} = 0.493E_2$, and $\nu_{12} = 0.32$. For the four-layer laminates, two different through thickness delamination locations, namely, midplane delamination ($h_2/h = 0.5$) and thinner delamination ($h_2/h = 0.25$), are considered for the analysis.

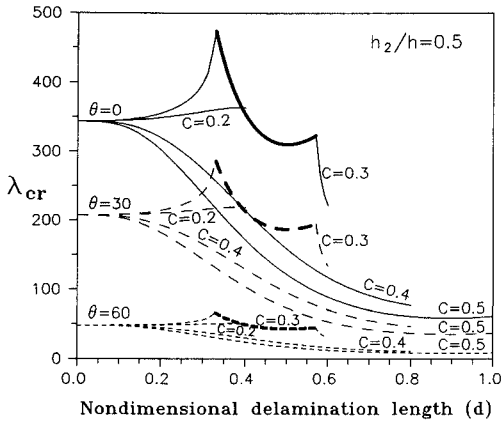

Fig. 2 Flutter boundary vs delamination length ($h_2/h = 0.5$).

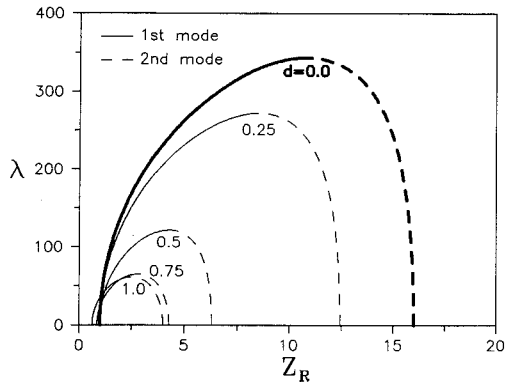

Fig. 3 Dynamic pressure vs eigenvalue ($\theta = 0$ deg, $c = 0.5$, $h_2/h = 0.5$).

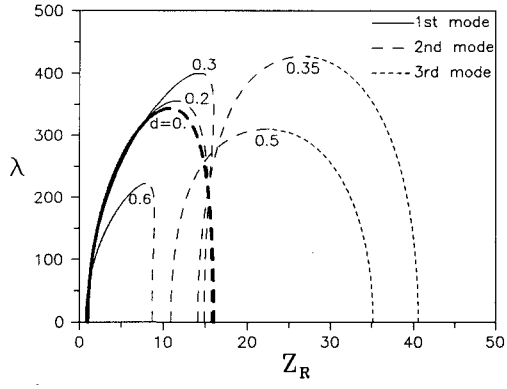

Fig. 4 Dynamic pressure vs eigenvalue ($\theta = 0$ deg, $c = 0.3$, $h_2/h = 0.5$).

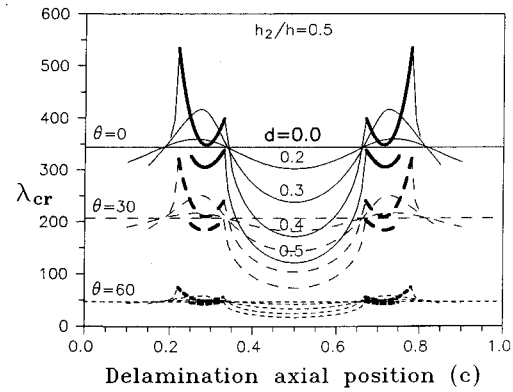

Fig. 5 Flutter boundary vs delamination axial position ($h_2/h = 0.5$).

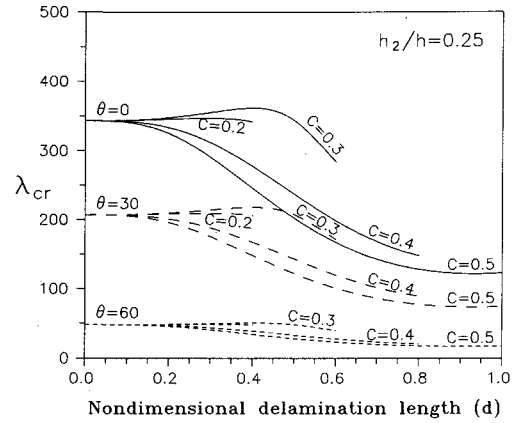

Fig. 6 Flutter boundary vs delamination length ($h_2/h = 0.5$).

Angle-Ply Laminates

Figure 2 shows the effect of midplane delamination length on the flutter boundaries of angle-ply laminates with three different fiber angles ($\theta = 0$, 30, and 60 deg) and four delamination axial positions ($c = 0.2$, 0.3, 0.4, and 0.5). It is seen that rotating fibers away from the x axis results in a reduction of the plate's stiffness in the x direction. Hence, the flutter boundary is in inverse proportion to the fiber angle. But the variation of the flutter boundary vs delamination length is the same for all fiber orientations. In general, for most delamination cases, the frequency coalescence occurs through the coupling of the first and second modes of the plate. Because the reduction in the natural frequencies by the delamination increases with the delamination length and the delamination reduces the mode 2 frequency much more rapidly than the mode 1 frequency, the flutter boundary decreases with the increase of the delamination length. This situation can also be observed from the frequency coalescence plot shown in Fig. 3 for 0-deg angle-ply laminate with midplane delamination centered at $0.5a$. Enlarging the delamination will significantly lower the mode 2 frequency but only slightly reduce the mode 1 frequency; thus the two modes will move closer to each other as the delamination length increases. Once the two modes are close to each other, they will coalesce at a lower value of λ.

When the delamination moves toward the supported edges ($c = 0.2$ and 0.3), the effect of the delamination on the flutter

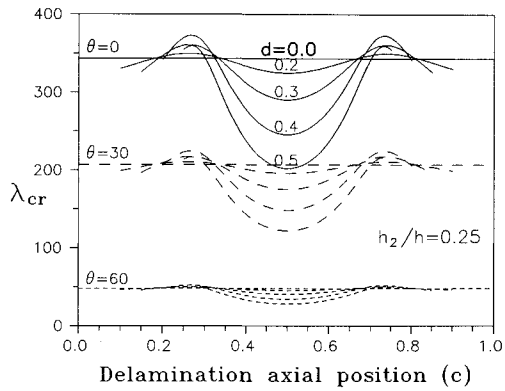

Fig. 7 Flutter boundary vs delamination axial position (h_2/h = 0.25).

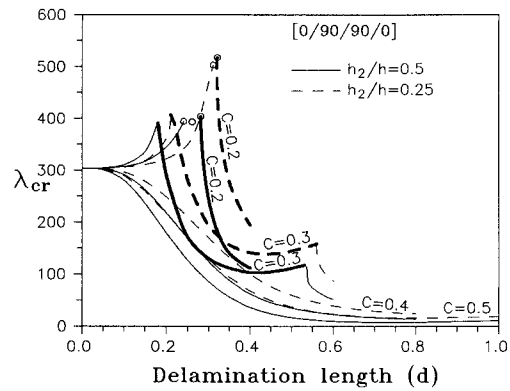

Fig. 8 Flutter boundary vs delamination length, [0/90/90/0].

boundary becomes different. The presence of the delamination may increase the flutter boundary. From the frequency coalescence analysis shown in Fig. 4 for 0-deg laminate, one can attribute this increase to the following: 1) the effect of the delamination on the mode 2 frequency is now not so significant; 2) although the frequency coalescence occurs between modes 1 and 2, the second mode has a tendency to coalesce with the third mode (i.e., the curve of the second mode bends toward the third mode as the flow velocity increases from zero; see Fig. 4 for $d = 0.3$ case). For the midplane delamination case with $c = 0.3$, the frequency coalescent pair shifts from modes 1 and 2 to modes 2 and 3 when the delamination length is between $0.33a$ and $0.57a$ (heavy thick line in Fig. 2). In this situation, the increase in the delamination length will decrease the flutter boundary due to the effect of the delamination on the mode 3 frequency higher than that on the mode 2 frequency (see Fig. 4 for $d = 0.35$ and 0.5 cases). As the delamination length is further enlarged over $0.57a$, the coalescent pair shifts back to modes 1 and 2 and the flutter boundary is also dropped sharply (see Fig. 4 for $d = 0.6$ case).

Figure 5 shows the effects of delamination axial position on the flutter boundary for the midplane delamination case. For all delamination length cases, the delamination has maximum destabilizing effect on the flutter boundary when the delamination centers at midspan. The effect of the delamination reduces quickly as the delamination moves away from the midspan region. The delamination may increase the flutter boundary when it centers at a location between $0.18a$–$0.34a$ or $0.66a$–$0.82a$ for the cases with shorter delamination length. It is also seen that, for $d = 0.4$ and 0.5 cases, the frequency coalescence occurs between modes 2 and 3 when the delamination centers from one-quarter to one-third span of the plate (heavy thick lines shown in Fig. 5).

Figures 6 and 7 show the effects of the delamination length and the delamination axial position on the flutter boundary of angle-ply laminates with thinner delamination. In general, the delamination has a similar effect on the flutter boundary as that on the cases with midplane delamination, except that the effect is smaller and there is no shift of frequency coalescent pair from modes 1 and 2 to modes 2 and 3. Hence, the plots of the flutter boundary vs delamination length or delamination axial position in Figs. 6 and 7 are more gradual than those in Figs. 2 and 5. The cause of these differences is mainly due to the ratio of bending stiffness of the delaminated portion of the plate to that of the undelaminated portion. The ratio is 0.25 for the midplane delamination case and 0.4375 for the thinner delamination case. With higher bending stiffness ratio, the effect of the delamination on the flutter boundary will be lower.

Cross-Ply Laminates

For cross-ply laminates with [0/90/90/0] construction, the bending stiffness of the delaminated portion of the plate is reduced significantly by the delamination. The bending stiffness ratios are 0.0669 and 0.1067, respectively, for midplane and thinner delamination cases that are much smaller than those for the corresponding cases of angle-ply laminates. Hence, the delamination now has a considerable effect on the flutter boundary.

Figure 8 shows the plot of the flutter boundary as a function of the delamination length with several delamination axial positions. Although the variations of the flutter boundary vs delamination length are similar to those in Figs. 2 and 6, there are several differences between the plots. First, the shifting of coalescent pair of eigenvalues for cross-ply laminates not only occurs in the case with delamination centered at $c = 0.3$ but also in the case with delamination centered at $c = 0.2$. Second, with certain delamination length centered at $c = 0.2$, the frequency coalescence occurs through the coupling of the third and fourth modes of the plate (open circle symbol in Fig. 8).

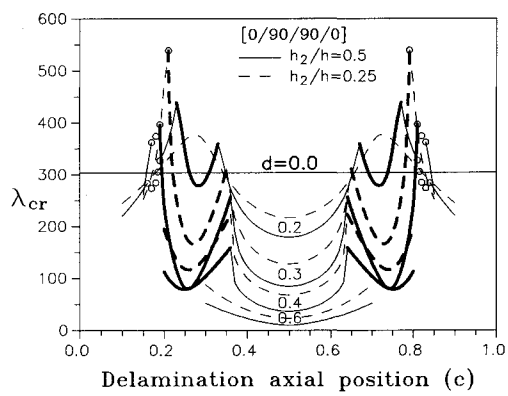

Fig. 9 Flutter boundary vs delamination axial position, [0/90/90/0].

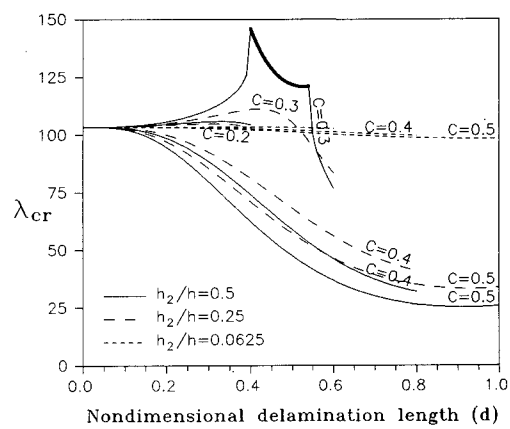

Fig. 10 Flutter boundary vs delamination length, $[(90, \pm 45, 0)_2]_{sym}$.

Finally, since the bending stiffness ratio of the thinner delaminated plate is low, the shifting of coalescent pair of eigenvalues is also evident in this case.

Figure 9 shows the effect of the delamination axial position on the flutter boundary of the [0/90/90/0] laminate. Similar to the cases for angle-ply laminates, the delamination has maximum destabilizing effect on the flutter boundary when the delamination centers at the midspan. As the delamination moves farther away from the midspan region, the coalescent pair of eigenvalues changes from modes 1 and 2 to modes 2 and 3 for cases with shorter or median delamination length (heavy thick lines in Fig. 9). Under this situation, the flutter boundary begins to drop sharply because the mode 3 frequency is reduced by the delamination much more rapidly than the mode 2 frequency. The lowest flutter boundary occurs in the range of $c = 0.25$–0.3 for all delamination lengths. Beyond this region, the flutter boundary rises again until the frequency coalescent pair shifts back to modes 1 and 2. The frequency coalescence may also occur through the coupling of modes 3 and 4 for the case with certain combinations of the delamination length and axial position (open circle in Fig. 9), but this kind of coalescence appears to have no significant effect on the variation of the flutter boundary curves.

Quasi-Isotropic Laminates $[(90, \pm 45, 0)_2]_{sym}$

In the preceding analyses only four-layer laminates were considered. In this section, a 16-layer laminate is examined. The $[(90, \pm 45, 0)_2]_{sym}$ is known as a quasi-isotropic laminate that is frequently used in current aerospace designs. The bending stiffness ratio is 0.327 for midplane delamination and gradually increases as the delamination moves up or down along the thickness direction. The maximum ratio is 0.9595 when the delamination is located next to the top or bottom layer. Because of the high bending stiffness ratios of the plate, the effect of the delamination on the flutter boundary becomes rather small.

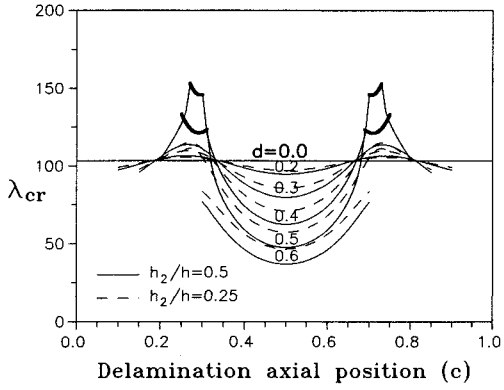

Fig. 11 Flutter boundary vs delamination axial position, $[(90, \pm 45, 0)_2]_{sym}$.

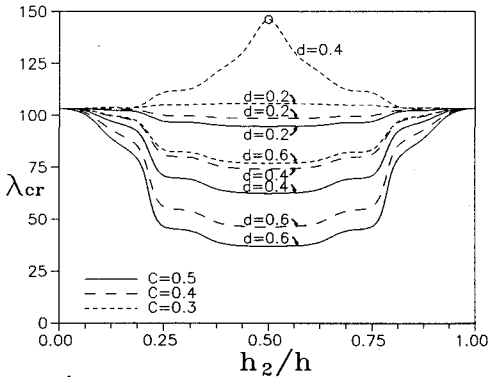

Fig. 12 Flutter boundary vs delamination location, $[(90, \pm 45, 0)_2]_{sym}$.

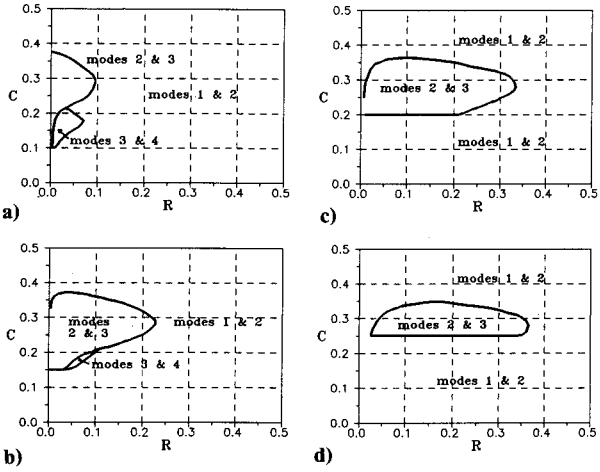

Fig. 13 Frequency coalescent pair range: a) $d = 0.2$, b) $d = 0.3$, c) $d = 0.4$, d) $d = 0.5$.

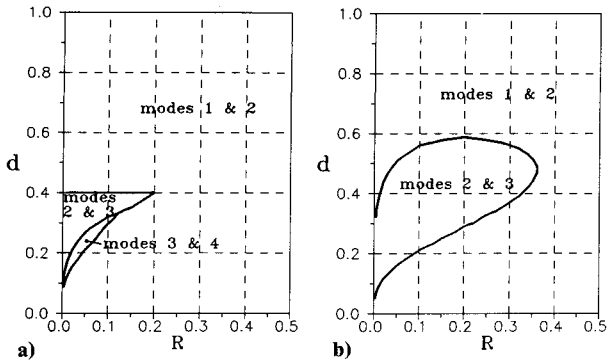

Fig. 14 Frequency coalescent pair range: a) $c = 0.2$, b) $c = 0.3$.

Some illustrative results for this laminate are displayed in Figs. 10 and 11. Figure 10 presents the effect of delamination length on the flutter boundary with four delamination axial positions and three through thickness locations. Figure 11 presents the effect of delamination axial position on the flutter boundary with six delamination lengths and two through thickness locations. Since the laminate is composed of 16 layers, it is of interest to see the variation of the flutter boundary as the delamination moves from the top of the plate to the bottom. Figure 12 presents the plot of the flutter boundary as a function of the through thickness location of the delamination. It shows that the presence of a delamination has a destabilizing effect on the flutter boundary for most of the cases, and the midplane delamination has the maximum effect due to its low bending stiffness ratio. However, the delamination may increase the flutter boundary when it centers at $0.3a$ and has length equal to $0.4a$. This is because the second mode of the plate has a tendency to coalesce with the third mode as the flow velocity increases. The open circle shown in the figure represents the case where the frequency coalescent pair are modes 2 and 3.

Effect of Bending Stiffness Ratio

Based on the preceding discussions, one can find that the bending stiffness ratio R of the delaminated portion of the plate to the undelaminated portion plays an important role in the determination of the flutter boundary and the frequency coalescent pair. From Eqs. (2), the bending stiffness ratio can be written as

$$R = \frac{D_2 + D_3}{D_1} - \frac{B_2^2}{D_1 A_2} - \frac{B_3^2}{D_1 A_3} \tag{17}$$

The range of R for isotropic material is from 0.25 to 1.0. For laminates considered in this study, the range of R is from 0.067 to 1.0. If $R > 0.5$, based on the preceding results, one

can say that the frequency coalescent pair of the eigenvalues is always modes 1 and 2. For $R < 0.5$, the frequency coalescence may occur between modes 2 and 3 or modes 3 and 4, depending on the size and location of the delamination. It is thus interesting to note that the range of R and the ranges of d and c for different frequency coalescent pairs may occur. With fixed delamination axial position c, Fig. 13 shows the ranges of R and d at which different coalescent pairs may occur. On the other hand, with fixed delamination length, Fig. 14 shows the ranges of R and c at which different coalescent pairs may occur.

Conclusions

A simple two-dimensional beam-plate model has been developed to study the effect of delamination on the supersonic flutter characteristics of a composite laminated beam plate. The parameters studied include location and size of the delamination and fiber orientation and stacking sequency of the laminates. Based on the present results, the following conclusions can be made:

1) For shorter delamination length (less than 20% of the plate span), the delamination has a moderate effect on the flutter performance. For delamination length longer than 20% of the plate span, the delamination has a pronounced destabilizing effect on the flutter performance of the plate if the location of the delamination centers near midspan.

2) When the delamination centers at a location from $0.2a$ to $0.35a$, it may increase the flutter boundary provided the delamination length is not too long.

3) Midplane delamination has the maximum destabilizing effect on the flutter performance of the plate.

4) The frequency coalescence usually occurs between the first two modes. However, for certain delamination location and size, the pair may shift from modes 1 and 2 to modes 2 and 3 or modes 3 and 4.

5) The bending stiffness ratio plays an important role in the determination of the flutter boundary and the frequency coalescent pair.

6) The simple beam-plate model can be used to evaluate the effects of delamination on the flutter boundary of a two-dimensional plate, and the results obtained using this model can also give the trends of the effects of delamination for comparison purposes.

Appendix: Elements in Matrix [K]

The nonzero elements of the [K] matrix are listed next:

$$K_{1,1} = K_{1,2} = K_{1,3} = K_{1,4} = 1$$

$$K_{2,1} = b_1^2 \qquad K_{2,2} = b_2^2 \qquad K_{2,3} = b_3^2 \qquad K_{2,4} = b_4^2$$

$$K_{3,9} = e^{b_1} \qquad K_{3,10} = e^{b_2} \qquad K_{3,11} = e^{b_3} \qquad K_{3,12} = e^{b_4}$$

$$K_{4,9} = b_1^2 e^{b_1} \qquad K_{4,10} = b_2^2 e^{b_2} \qquad K_{4,11} = b_3^2 e^{b_3} \qquad K_{4,12} = b_4^2 e^{b_4}$$

$$K_{5,1} = e^{b_1 s_1} \qquad K_{5,2} = e^{b_2 s_1} \qquad K_{5,3} = e^{b_3 s_1} \qquad K_{5,4} = e^{b_4 s_1}$$

$$K_{5,5} = -e^{\bar{b}_1 s_1} \qquad K_{5,6} = -e^{\bar{b}_2 s_1} \qquad K_{5,7} = -e^{\bar{b}_3 s_1} \qquad K_{5,8} = -e^{\bar{b}_4 s_1}$$

$$K_{6,1} = b_1 e^{b_1 s_1} \qquad K_{6,2} = b_2 e^{b_2 s_1} \qquad K_{6,3} = b_3 e^{b_3 s_1} \qquad K_{6,4} = b_4 e^{b_4 s_1}$$

$$K_{6,5} = -\bar{b}_1 e^{\bar{b}_1 s_1} \qquad K_{6,6} = -\bar{b}_2 e^{\bar{b}_2 s_1} \qquad K_{6,7} = -\bar{b}_3 e^{\bar{b}_3 s_1} \qquad K_{6,8} = -\bar{b}_4 e^{\bar{b}_4 s_1}$$

$$K_{7,5} = -e^{\bar{b}_1 s_2} \qquad K_{7,6} = -e^{\bar{b}_2 s_2} \qquad K_{7,7} = -e^{\bar{b}_3 s_2} \qquad K_{7,8} = -e^{\bar{b}_4 s_2}$$

$$K_{7,9} = e^{b_1 s_2} \qquad K_{7,10} = e^{b_2 s_2} \qquad K_{7,11} = e^{b_3 s_2} \qquad K_{7,12} = e^{b_4 s_2}$$

$$K_{8,5} = -\bar{b}_1 e^{\bar{b}_1 s_2} \qquad K_{8,6} = -\bar{b}_2 e^{\bar{b}_2 s_2} \qquad K_{8,7} = -\bar{b}_3 e^{\bar{b}_3 s_2} \qquad K_{8,8} = -\bar{b}_4 e^{\bar{b}_4 s_2}$$

$$K_{8,9} = b_1 e^{b_1 s_2} \qquad K_{8,10} = b_2 e^{b_2 s_2} \qquad K_{8,11} = b_3 e^{b_3 s_2} \qquad K_{8,12} = b_4 e^{b_4 s_2}$$

$$K_{9,1} = b_1^3 e^{b_1 s_1} \qquad K_{9,2} = b_2^3 e^{b_2 s_1} \qquad K_{9,3} = b_3^3 e^{b_3 s_1} \qquad K_{9,4} = b_4^3 e^{b_4 s_1}$$

$$K_{9,5} = \bar{A}\bar{b}_1^3 e^{\bar{b}_1 s_1} \qquad K_{9,6} = \bar{A}\bar{b}_2^3 e^{\bar{b}_2 s_1} \qquad K_{9,7} = \bar{A}\bar{b}_3^3 e^{\bar{b}_3 s_1} \qquad K_{9,8} = \bar{A}\bar{b}_4^3 e^{\bar{b}_4 s_1}$$

$$K_{10,5} = \bar{A}\bar{b}_1^3 e^{\bar{b}_1 s_2} \qquad K_{10,6} = \bar{A}\bar{b}_2^3 e^{\bar{b}_2 s_2} \qquad K_{10,7} = \bar{A}\bar{b}_3^3 e^{\bar{b}_3 s_2} \qquad K_{10,8} = \bar{A}\bar{b}_4^3 e^{\bar{b}_4 s_2}$$

$$K_{10,9} = b_1^3 e^{b_1 s_2} \qquad K_{10,10} = b_2^3 e^{b_2 s_2} \qquad K_{10,11} = b_3^3 e^{b_3 s_2} \qquad K_{10,12} = b_4^3 e^{b_4 s_2}$$

$$K_{11,1} = b_1^2 e^{b_1 s_1} \qquad K_{11,2} = b_2^2 e^{b_2 s_1} \qquad K_{11,3} = b_3^2 e^{b_3 s_1} \qquad K_{11,4} = b_4^2 e^{b_4 s_1}$$

$$K_{11,5} = (\bar{A}\bar{b}_1 - \bar{B})\bar{b}_1 e^{\bar{b}_1 s_1} + \bar{B}\bar{b}_1 e^{\bar{b}_1 s_2} \qquad K_{11,6} = (\bar{A}\bar{b}_2 - \bar{B})\bar{b}_2 e^{\bar{b}_2 s_1} + \bar{B}\bar{b}_2 e^{\bar{b}_2 s_2}$$

$$K_{11,7} = (\bar{A}\bar{b}_3 - \bar{B})\bar{b}_3 e^{\bar{b}_3 s_1} + \bar{B}\bar{b}_3 e^{\bar{b}_3 s_2} \qquad K_{11,8} = (\bar{A}\bar{b}_4 - \bar{B})\bar{b}_4 e^{\bar{b}_4 s_1} + \bar{B}\bar{b}_4 e^{\bar{b}_4 s_2}$$

$$K_{12,5} = (\bar{A}\bar{b}_1 - \bar{B})\bar{b}_1 e^{\bar{b}_1 s_2} + \bar{B}\bar{b}_1 e^{\bar{b}_1 s_1} \qquad K_{12,6} = (\bar{A}\bar{b}_2 + \bar{B})\bar{b}_2 e^{\bar{b}_2 s_2} - \bar{B}\bar{b}_2 e^{\bar{b}_2 s_1}$$

$$K_{12,7} = (\bar{A}\bar{b}_3 - \bar{B})\bar{b}_3 e^{\bar{b}_3 s_2} + \bar{B}\bar{b}_3 e^{\bar{b}_3 s_1} \qquad K_{12,8} = (\bar{A}\bar{b}_4 + \bar{B})\bar{b}_4 e^{\bar{b}_4 s_2} - \bar{B}\bar{b}_4 e^{\bar{b}_4 s_1}$$

$$K_{12,9} = b_1^2 e^{b_1 s_2} \qquad K_{12,10} = b_2^2 e^{b_2 s_2} \qquad K_{12,11} = b_3^2 e^{b_3 s_2} \qquad K_{12,12} = b_4^2 e^{b_4 s_2}$$

where

$$\bar{A} = \left[\frac{B_2^2}{D_1 A_2} + \frac{B_3^2}{D_1 A_3} - \frac{(D_2 + D_3)}{D_1}\right]$$

$$\bar{B} = \left(\frac{B_2}{A_2} - \frac{B_3}{A_3}\right)\left[\frac{A_2 B_3 - A_3 B_2}{D_1(s_2 - s_1)(A_2 + A_3)}\right]$$

References

[1]Tracy, J. J., and Pardoen, G. C., "Effect of Delamination on the Natural Frequencies of Composite Laminates," *Journal of Composite Materials,* Vol. 23, 1989, pp. 1200–1215.

[2]Simitses, G. J., Sallam, S., and Yin, W. L., "Effect of Delamination of Axially Loaded Homogeneous Laminated Plates," *AIAA Journal,* Vol. 23, No. 9, 1985, pp. 1437–1444.

[3]Yin, W. L., Sallam, S. N., and Simitses, G. J., "Ultimate Axial Load Capacity of a Delaminated Beam-Plate," *AIAA Journal,* Vol. 24, No. 1, 1986, pp. 123–128.

[4]Dowell, E. H., "Nonlinear Oscillations of a Fluttering Plate," *AIAA Journal,* Vol. 4, No. 7, 1966, pp. 1267–1275.

[5]Dowell, E. H., "Nonlinear Oscillations of a Fluttering Plate II," *AIAA Journal,* Vol. 5, No. 10, 1967, pp. 1856–1862.

[6]Ventres, C. S., and Dowell, E. H., "Comparison of Theory and Experiment for Nonlinear Fluttering of Loaded Plates," *AIAA Journal,* Vol. 8, No. 11, 1970, pp. 2022–2030.

[7]Eastep, F. E., and McIntosh, S. C., "Analysis of Nonlinear Panel Flutter and Response Under Random Excitation or Nonlinear Aerodynamic Loading," *AIAA Journal,* Vol. 9, No. 3, 1971, pp. 411–418.

[8]Morino, L., "A Perturbation Method for Treating Nonlinear Panel Flutter Problems," *AIAA Journal,* Vol. 7, No. 3, 1969, pp. 405–411.

[9]Kuo, C. C., Morino, L., and Dugundji, J., "Perturbation and Harmonic Balance Methods for Nonlinear Panel Flutter," *AIAA Journal,* Vol. 10, No. 11, 1972, pp. 1479–1484.

[10]Smith, L., and Morino, L., "Stability Analysis of Nonlinear Differential Antonomous Systems with Applications to Flutter," *AIAA Journal,* Vol. 14, No. 3, 1976, pp. 333–341.

[11]Mei, C., "A Finite Element Approach for Nonlinear Panel Flutter," *AIAA Journal,* Vol. 15, No. 8, 1977, pp. 1107–1110.

[12]Rao, K. S., and Rao, G. V., "Large Amplitude Supersonic Flutter of Panels with Ends Elastically Restrained Against Rotation," *Computers and Structures,* Vol. 11, 1980, pp. 197–201.

[13]Han, A. D., and Yang, T. Y., "Nonlinear Panel Flutter Using High-Order Triangular Finite Element," *AIAA Journal,* Vol. 21, No. 10, 1983, pp. 1453–1461.

[14]Sarma, B. S., and Varadan, T. K., "Nonlinear Panel Flutter by Finite Element Method," *AIAA Journal,* Vol. 26, No. 5, 1988, pp. 566–574.

[15]Dowell, E. H., "Flutter of a Buckled Plate as an Example of Chaotic Motion of a Deterministic Autonomous System," *Journal of Sound and Vibration,* Vol. 85, 1982, pp. 333–344.

[16]Ketter, D. J., "Flutter of Flat Rectangular Orthotropic Panels," *AIAA Journal,* Vol. 5, No. 1, 1967, pp. 116–124.

[17]Rossettos, J. W., and Tong, P., "Finite Element Analysis of Vibration and Flutter of Cantilever Anisotropic Plates," *Journal of Applied Mechanics,* Vol. 41, No. 4, 1974, pp. 1075–1080.

[18]Sawyer, J. W., "Flutter and Buckling of General Laminated Plates," *Journal of Aircraft,* Vol. 14, No. 4, 1977, pp. 387–393.

[19]Shiau, L. C., and Lu, L. T., "Nonlinear Flutter of Two-Dimensional Simply Supported Symmetric Composite Laminated Plates," *Journal of Aircraft,* Vol. 29, No. 1, 1992, pp. 140–145.

[20]Shiau, L. C., and Chang, J. T., "Transverse Shear Effect on Flutter of Composite Panels," *Journal of Aerospace Engineering* (to be published).